A semisynthetic peptide-metalloporphyrin responsive matrix for artificial photosynthesis

Sun, Z.

Chapter 2

Self-assembly of a semisynthetic zinc-protoporphyrin IX peptide complex derived from the natural CsmA light harvesting antenna

2.0 Abstract

The CsmA protein from the baseplate of the *Chlorobaculum tepidum* is proposed as an attractive motif for the engineering of semisynthetic materials for artificial photosynthesis. We perform self-assembly of zinc protoporphyrin IX (ZnPP) with a truncated CsmA (tCsmA) amphipathic peptide scaffold for the bottom-up construction of a semisynthetic matrix for energy transfer. The resulting self-assembly shows an extended periodic structure with 7_2 helical symmetry. The complex is able to maintain a good photostability for at least 30 min when the concentration is more than 20 µM, and almost 100% harvested energy can be transferred to the acceptor cation radical methyl viologen (MV^+). The excitation-energy transfer rate of the complex was increased from the ns^{-1} scale to the ps^{-1} scale that is comparable to natural light-harvesting antenna systems. It contributes to converging evidence that chiral responsive matrix assemblies can be developed for efficient light energy harvesting in artificial photosynthesis.

This chapter has been published as: Zhongwu Sun, Christoph A. Diebolder, Ludovic Renault, Huub de Groot. A semisynthetic peptide-metalloporphyrin responsive matrix for artificial photosynthesis, 2019, *ChemPhotoChem*

2.1 Introduction

Solar energy is a major source of renewable energy with the potential to address major sustainability challenges the world is facing. A finite supply of low carbon electricity from photovoltaics and wind can be followed by electrolysis to produce fuels, but such adiabatic conversion and concentration chains are not optimally efficient. In contrast, nature makes abundant use of non-adiabatic conversions that transiently violate detailed balance for high yield.[1-3] Photosynthesis uses ordered arrays of pigments for energy or charge transfer.[4-5] Traditionally, transmission of exciton energy is thought to proceed via the Förster or Dexter exciton transfer mechanisms.[6-8] However, photosynthetic proteins are chiral matrix assemblies which are thought to undergo a light-driven conformational change and self-select vibrations to develop vibronic states for driving semi-classical coherent transfer with nearly 100% yield in lossless processes, a concept known as the responsive matrix.[9-13]

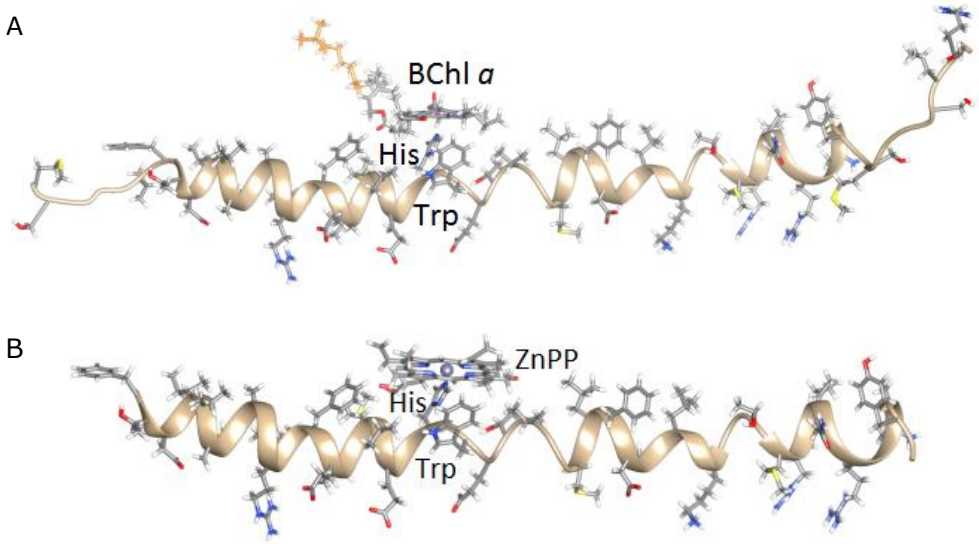

Figure 2.1 (A) The structure of the CsmA-BChl *a* complex from the baseplate (PDB 5LCB). (B) Putative model structure of the tCsmA in complex with ZnPP, as derived from the CsmA-BChl *a* complex.

The critical step in constructing a responsive matrix is the chemical engineering of a chiral module. Here we start from a zinc protoporphyrin IX (ZnPP) chromophore and provide a new paradigm for energy transfer in a semi-synthetic matrix for artificial photosynthesis.[14-16] We use tCsmA

construct, containing 43 amino acids, which is derived from the helical CsmA peptide from the baseplate of *Chlorobaculum tepidum*. This is the smallest light-harvesting protein known in nature, and coordinates a single BChl *a* (Figure 2.1B). The tCsmA was modified by removing the flexible segments from the N and C-terminal, which attach to the lipid monolayer confining the chromosome and the FMO complex respectively, leaving the functional central α-helix.[17] In nature, dimers of CsmA-BChl *a* self-assemble to form extended para-crystalline layers with BChl *a* in CsmA strands.[17] The system assists in energy transfer and storage from the chlorosome to the FMO antenna and the photosynthetic reaction center in *Chlorobaculum tepidum* (Figure 1.2).[18-19] NMR studies of monomeric CsmA in solution have shown that it is a α-helical amphipathic peptide.[20] With the exception of the single coordinating histidine in the sequence, all potentially charged residues, like glutamine, lysine and arginine, are located on one side of the helix (Figure 1.3 & 2.1A).

With the assistance of tCsmA scaffolds, ZnPP (SFigure 2.1) is bound to form a molecular wire with complexation via slow dialysis.[21] We perform initial assays of the light harvesting, indicating that excitons formed in the array upon photoexcitation have lifetimes on the ns scale, comparable to ZnPP in solution.[22] When energy transfer is significantly faster than this, a high efficiency of energy transfer can be obtained.[23] When a quencher methyl viologen (MV) is used in excess to accept the harvested light energy from ZnPP, nearly 100% of the fluorescence is rapidly quenched, consistent with a high efficiency of excitation-energy transfer from the ZnPP wires to the MV.[24-28]

2.2 Experimental section

2.2.1 Materials

Zn(II) Protoporphyrin IX (ZnPP) was purchased from Frontier Scientific. The tCsmA, with N-Terminal Acetylation and C-Terminal Amidation, was purchased from GL Biochem Ltd (98% purity). Dimethyl sulfoxide (DMSO, Sigma Aldrich), monobasic dihydrogen phosphate (Sigma Aldrich), dibasic monohydrogen phosphate (Sigma Aldrich), 1-propanol (Sigma Aldrich) and the microdialysis vial (Pierce™ 96-well Microdialysis Plate, 3.5K MWCO, Thermo Fisher Scientific) were used for constitution of tCsmA-ZnPP

complexes. MV and sodium dithionite (85% purity) were obtained from Sigma-Aldrich.

2.2.2 Equipments

The concentration of protein was measured with a Microvolume DS-11 Spectrophotometer (DeNovix). The steady state Fluorescence spectra were measured using a FLS900 Fluorescence Spectrometer (Edinburgh Instruments) and Aqualog® Water Treatment Plant Analyzer (HORIBA Scientific). The UV-Vis spectra were measured using a UV-1700 Spectrophotometer (Shimadzu). The molar extinction coefficient of the complex was determined by Vista MPX Simultaneous Inductive Coupled Plasma-Optical Emission Spectrometry (ICP-OES, Varian Inc.). The complex was loaded with a 10 µL injection loop on a SuperdexTM 200 Increase 5/150 GL column (GE Healthcare) to perform Size-Exclusion Chromatography (SEC). Negative stain images were obtained with a JEM-1010 transmission electron microscope with a maximum output voltage up to 70 KV equipped with an Olympus Megaview camera (JEOL Ltd.). The circular Dichroism (CD) spectra were measured using a J-815 CD spectrometer (JASCO). The Linear Dichroism (LD) spectra were measured using a Chirascan CD Spectrophotometer (Applied Photophysics). The time-resolved fluorescence measurements were performed with a FluoTime 300 instrument (PicoQuant).

2.2.3 Methods

The peptide was synthesized using standard solid-phase Fmoc based chemistry and purified by RP-HPLC from GL Biochem Ltd (98% purity). To ensure the similar biological activity with natural CsmA, the modification of N-Terminal Acetylation and C-Terminal Amidation were included. The sequence of the peptide corresponds to residues 7-49 of CsmA:
Ac-FTDILAAAGRIFEVMVEGHWETVGMLFDSLGKGTMRINRNAYG-NH_2

Constitution of the tCsmA-ZnPP complex was carried out in a molar ratio 5:1 mixture of ZnPP and tCsmA dissolved in pH 7.9 50 mM Potassium Phosphate buffer (KPi buffer) containing 6M 1-propanol. The ZnPP was added from a 200 mM DMSO solution. The reaction proceeded in the microdialysis vial against 4 times 1.4 mL KPi dialysis buffer at 4 °C in the dark. The dialysis

times were 2 hours except for the third one, where the sample was incubated overnight. After the last dialysis step, the sample volume was increased from 100 µL to 130 µL and the sample was centrifuged for 15 minutes at 4 °C with 30,000 × *g* to remove unbound CsmA and ZnPP precipitate.

To determine the extinction coefficient, different concentrations of tCsmA-ZnPP complex solutions were prepared. For each aliquot the absorption at 430 nm was measured and the Zn concentration was determined by ICP-OES to calculate the extinction coefficient of the complex. By combining a Bicinchoninic Acid (BCA) assay with the molar extinction coefficient of the complex, the stoichiometry was determined.

To observe the particles by TEM, the tCsmA-ZnPP complex was loaded onto an EM grid with a layer of amorphous carbon film that was rendered hydrophilic by glow discharge (EMS K100X, Agar Scientific) for 1 min at 30 mA. After quick washing with 10 µL distilled water 2 times, 5 µL sample was applied to the grid and left for 30 seconds. Subsequently the sample was stained quickly with 10 µL 2% (w/v) uranyl acetate solution, followed by blotting of excess solution and air-drying.

For Cryo-EM, grids were prepared by placing 4 µL of 200 µM tCsmA-ZnPP complex in KPi buffer onto 200 mesh grids with 2 µm holes (Quantifoil R2/2, Quantifoil Micro Tools, GmbH). Grids were glow discharged for 20 seconds prior to plunge freezing in liquid ethane cooled by liquid nitrogen, using a FEI Vitrobot IV at 100% relative humidity, chamber temperature of 4 °C. Data were collected at 300 kV with a Titan Krios electron microscope, using an electron dose of 51 $e^{-}/Å^{2}$ and a magnification of 75,000×. The final object sampling was therefore 0.88 Å/pixel. Exposures were recorded using the EPU automated acquisition software on a FEI Falcon II direct electron detector. The single particle analysis was performed with Relion 2.0, while Fiji was used for Fourier transforms of 2D class images.

For the time-resolved fluorescence measurements, the samples were prepared with 500 µM MV, 1.25 mM sodium dithionite and tCsmA-ZnPP complex in KPi buffer or the monomeric ZnPP in 6 M propanol buffer. The excitation beam was 440 nm.

For LD experiments, a squeezing gel of 5% acrylamide with 50% glycerol was used (STable 2.2). To avoid fast degradation of the sample by components of the squeezing gel, the procedure was optimized. All materials were cooled on ice before use. To prepare the gel, all components except the sample were mixed, and put at room temperature for 2.5 minutes. The complex was added and the solution was transferred to the gel squeezer. The system was kept on ice for 5 minutes and another 5 minutes at room temperature and immediately the LD was measured.

For steady state fluorescence measurements, the samples were prepared with 1.25 mM sodium dithionite and tCsmA-ZnPP complex in KPi buffer or the monomeric ZnPP in 6 M propanol buffer, and with different concentrations of MV. The excitation wavelength was 430 nm for the tCsmA-ZnPP complex and 416 nm for ZnPP monomer. In addition, steady state fluorescence was measured for both samples with 440 nm excitation light, corresponding with the wavelength used in time-resolved fluorescence experiments.

2.3 Results and discussion

2.3.1 Constitution and characterization

An important finding of our studies is that slow dialysis is key to form a tCsmA-ZnPP complex, since the complex is moderately soluble while the components precipitate upon dialysis. The 1-propanol, which is thought to cover the hydrophobic side of randomly aggregated tCsmA, is slowly removed by dialysis against KPi buffer. This exposes the histidine, which is the only charged residue at the hydrophobic side and is the binding site for coordination to ZnPP. UV-vis spectroscopy indicates histidyl axial binding of the chromophore by characteristic bathochromic shifts around 15 nm relative to the monomeric ZnPP in solution (Figure 2.2A).[15, 29] As a control experiment, we performed dialysis of either the ZnPP or the tCsmA in 50 mM KPi buffer containing 6 M 1-propanol and it was found that both precipitate upon dialysis against KPi buffer (blue trace in Figure 2.2A). This suggests that dialysis should be slow compared to the binding to prevent precipitation of separate components. The B-band shifts by 14 nm, from 416 nm to 430 nm, while the Q(1,0) and Q(0,0) bands shift by 8 and 7 nm to 554 nm and 590 nm, respectively, after constitution (Figure 2.2A). These shifts

are well in line with literature data collected from semi-artificial systems, which consistently show shifts in the range of 10-15 nm for the B-band.[14, 30] After binding, the absorption in the Q(1,0) band of the tCsmA-ZnPP complex is stronger than for the Q(0,0) band, while for the ZnPP monomer the absorption for the Q(1,0) band is less than for the Q(0,0) band. The relative intensities of these bands correlate with the stability of the complex, and the decrease of the Q(0,0) band relative to the Q(1,0) band upon formation of the complex indicates that binding enhances the stability of the complex with a square-planar Zn^{2+} in the porphyrin.[31-32]

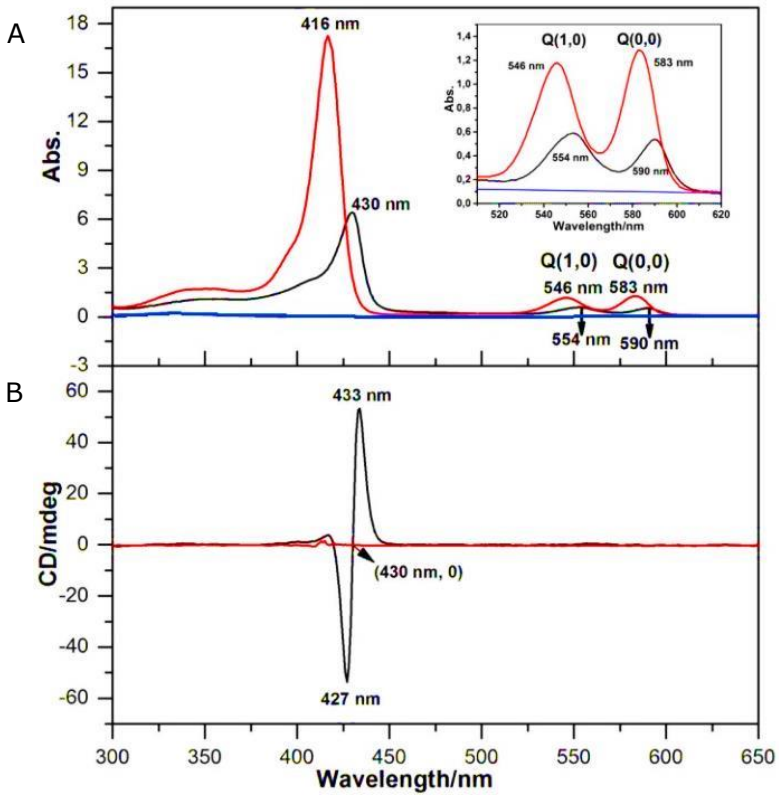

Figure 2.2 (A) UV-Vis and (B) corresponding CD spectra, collected from 50 µM tCsmA-ZnPP complex in 50 mM KPi buffer (black) and 50 µM ZnPP in 50 mM KPi buffer containing 6 M 1-propanol (red), respectively. The blue line shown in panel A is the residual UV response from KPi buffer after dialysis, *i.e.* without tCsmA, confirming that ZnPP has precipitated. The window of the enlarged Q bands region is shown in panel A. The concentration of peptide at the start of the dialysis is 50 mM in KPi buffer with 6 M 1-propanol and there is no CD response (B, red trace). Upon complex formation a CD response is detected (B, black trace).

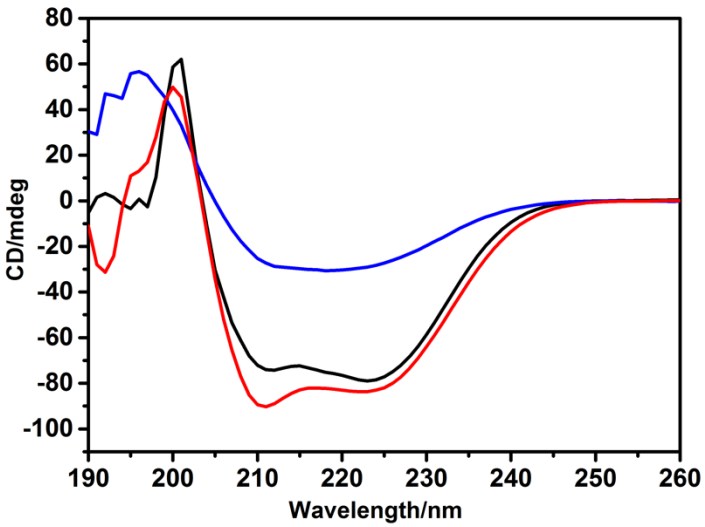

Figure 2.3 CD spectra. black: 50 µM tCsmA-ZnPP complex in pH 7.9 50 mM KPi buffer; red: 50 µM tCsmA in pH 7.9 6 M 1-propanol 50 mM KPi buffer. Both CD signals are characteristic for a helical secondary structure. In contrast, while the tCsmA possesses a maximum 50 µM solubility in MQ water, it shows a denatured β-sheet structure, and the binding cannot proceed in this condition (blue line). Samples were measured in quartz cuvettes with a 2 mm path length. Spectra were recorded from 260 to 190 nm at 1 nm intervals with a 1 nm bandwidth at 25 °C.

Moreover, the CD spectrum in Figure 2.3 for the secondary structure reveals the maintenance of a helical structure only when the ZnPP is bound. Therefore the slow dialysis is vitally important for the self-assembly of an intact helix structure with tCsmA bound to ZnPP.

Table 2.1 The concentration of zinc measured by ICP-OES with corresponding UV absorption at 430 nm

Zn (C,µM) Measured by ICP- OES	Complex Abs. at 430 nm
0.06295	0.070
0.82441	0.103
1.08106	0.147
1.30101	0.166
1.66412	0.210
2.02203	0.248
2.29428	0.266
2.59254	0.295
2.85408	0.322
3.12787	0.362

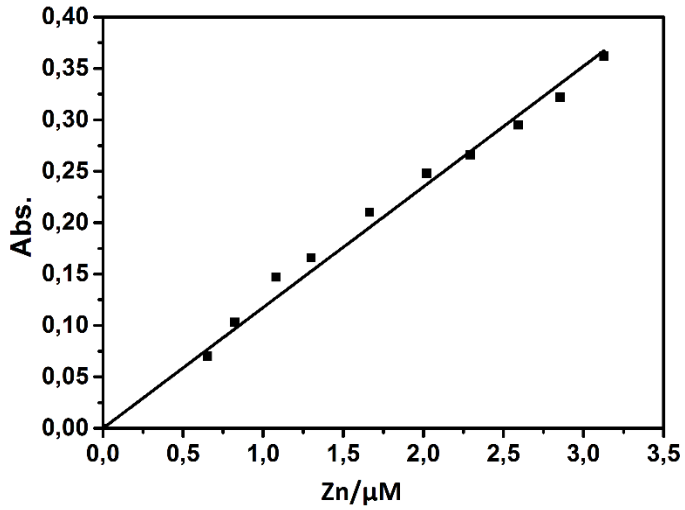

Figure 2.4 Standard curve represents the relationship between the Zn concentration in CsmA-ZnPP determined by ICP-OES and its absorbance maximum (λ = 430 nm). The resulting functional equation is Y = 0.1174X; R^2 = 0.9975.

The molar extinction coefficient ε can be determined using equation: ε = A / (c * l), which was converted based on the Beer-Lambert law, A = ε *c * l, where A represents an actual absorption at the given wavelength, path length l is 1 cm in our study, and the molar concentration c was obtained from the Zn concentration (C_{Zn}, µM) determined by ICP-OES. The molar extinction coefficient of the ZnPP in complex with tCsmA is 117400 M^{-1} cm^{-1} and was determined by the combined use of UV-Vis and ICP-OES (Table 2.1 & Figure 2.4).[34] With a subsequent BCA assay, a stoichiometry of tCsmA: ZnPP ~ 1 : 1 was determined (Table 2.2).

Table 2.2 The amount of protein in the complex was determined using the colorimetric BCA protein assay. The stoichiometry of complex can be calculated from the ratio of the protein concentration to the concentration of Zn.

ZnPP (C, µM) Measured from A430 nm	**tCsmA (C, µM) Measured by BCA assay**	**Ratio C_{ZnPP} / C_{tCsmA}**
13.8	13.6	1.01 ± 0.01
8.5	8.0	1.06 ± 0.02
3.3	3.5	0.94 ± 0.04

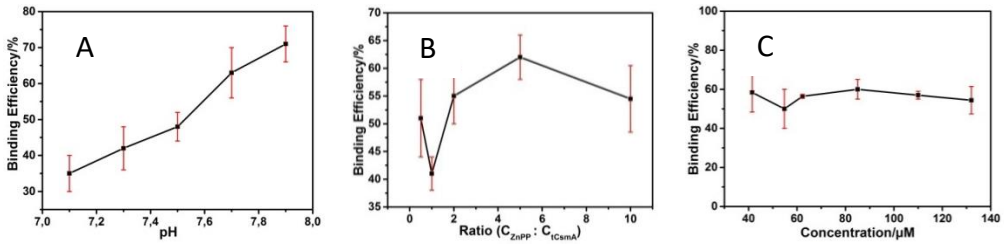

Figure 2.5 Optimization of the binding between CsmA and ZnPP during dialysis. A: The influence of the pH of KPi buffer (C_{tCsmA}=70 µM, C_{ZnPP}=350 µM). B: The influence of the ratio of CsmA and ZnPP in KPi pH 7.9 buffer (C_{tCsmA}=50 µM). C: The influence of the tCsmA concentration in KPi pH 7.9 buffer (C_{tCsmA} : C_{ZnPP}=1 : 5).

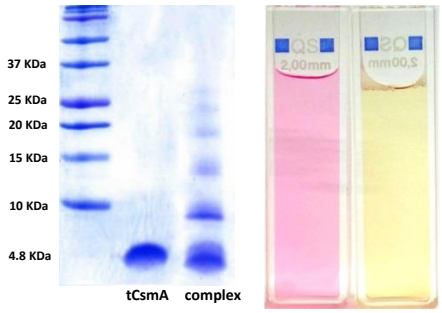

Figure 2.6 left: Tricine-SDS gel analysis of the complex and tCsmA. Prior to loading the samples were boiled for 4 min. Lane 1: Marker. Lane 2: tCsmA. Lane 3: the ZnPP-CsmA complex. right: cuvettes containing 50 µM ZnPP without tCsmA mixture in 6 M 1-propanol KPi buffer (left cuvette) and 50 µM tCsmA-ZnPP complex in KPi buffer (right cuvette).

At pH=7.9 and with five times molar excess of ZnPP relative to the concentration of peptide, the binding optimally proceeds, with an efficiency of ~ 60-70% over a peptide concentration range of 40-130 µM (Figure 2.5). UV-Vis spectra showed a narrow singlet peak at 430 nm, which indicates high purity. The concentration of protein has little influence on the binding efficiency. Similar to the natural CsmA-BChl *a* complex, the tCsmA-ZnPP complex shows oligomer bands on the SDS gel (Figure 2.6).[33] The complex is stable during three months storage in the dark at 4°C.

2.3.2 Structural information

Under cryo-conditions of TEM the images show long filaments (Figure 3A). We performed maximum likelihood 2D classification of 99142 particles using

a mask size of 535 Å, corresponding with a box size of 610 pixels. All 50 2D class averages show the same chain-like structure (SFigure 2.2).[17]

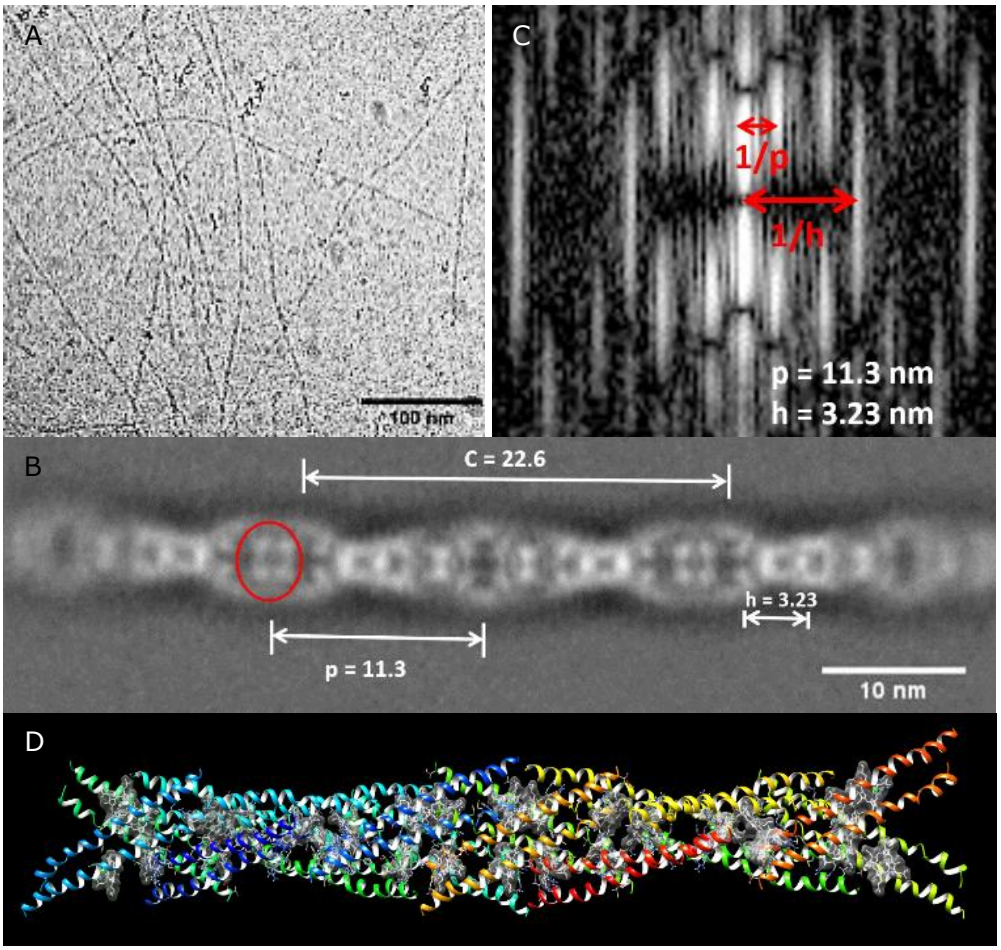

Figure 2.7 (A) cryo-EM image showing individual filaments in a sample of 200 µM tCsmA-ZnPP complex in KPi buffer. (B) 2D class average of particles from cryo-EM images. (C) Fast Fourier Transform of a 2D class average (Figure 3B). (D) Proposed assembly model according to the parameters from the 2D class average. Each subunit has a different colour and the ZnPP are depicted in light grey. Due to the image processing, there is a contrast inversion from A to B.

The diameter of a filament is about 5 nm (Figure 2.7B). As the Fast Fourier Transform (FFT) Figure 2.7C shows, multiple layer lines separated by 1/22.6 nm^{-1} provide converging and convincing evidence for a helical structure with a C= 22.6 ± 0.02 nm periodic repeat. The strongest peaks close to the meridian are on the second layer line, corresponding with a helix pitch p=11.3 ± 0.02 nm, *i.e.* half of the repeat (Figure 2.7C). The seventh layer line

with intensity on the meridian reveals a helical rise h=3.23 ± 0.02 nm, and according to the FFT the complex forms a 7_2 helix. A proposed assembly is shown in Figure 2.7D. The high density parts inside the filaments can be attributed to tetrameric units of tightly packed ZnPP (Figure 2.7B, labelled with the red circle). The size of the ZnPP clusters is ~ 1.2 nm, and they are separated by ~2 nm. In addition, most likely the system self-assembles as a symmetric double helix.

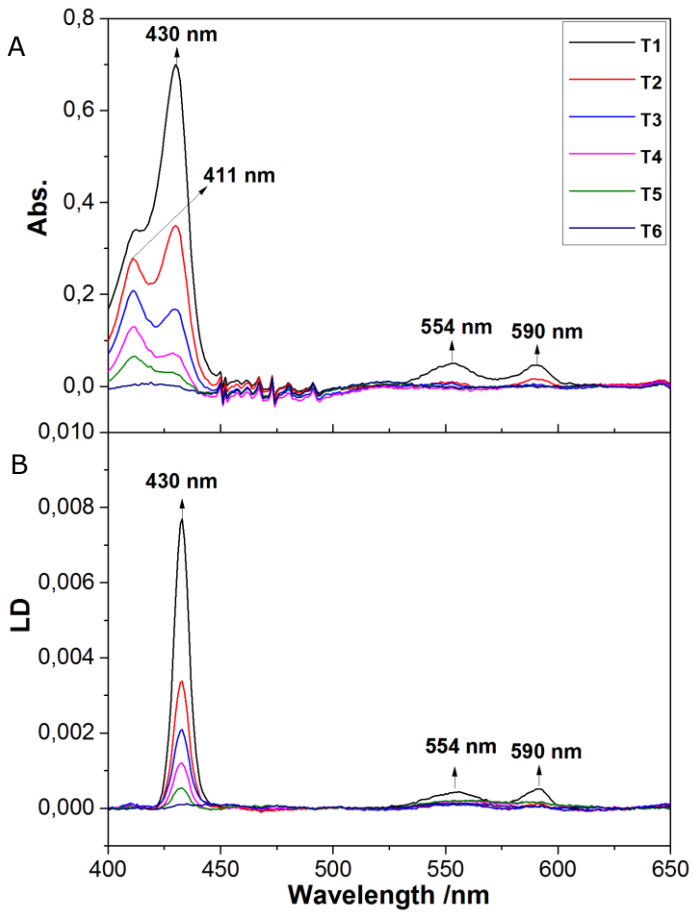

Figure 2.8 (A) UV-Vis and (B) corresponding LD spectra. The spectrum T1 corresponds to the first measurement, T2 was collected after 7 min, T3 after 13 min, T4 after 19 min, T5 after 30 min and T6 after 1 h 14 min.

Linear Dichroism (LD) allows to determine the macroscopic orientation from the absorption of parallel and perpendicular linearly polarized light, and to study the orientation of the ZnPP in the filaments, we collected LD data along with simultaneous UV-Vis absorbance spectra in a squeezing gel.

According to the UV-Vis results (Figure 2.8A), an additional 411 nm ZnPP peak appears, in contrast with the UV-Vis data collected from the complex in solution (black trace in Figure 2.2A). The shift to 411 nm is attributed to loss of binding and decomposition by squeezing gel components (Table 2.1, SFigure 2.4). The LD spectra measured over time show positive peaks at 430 nm with the two Q band signals at 554 nm and 590 nm, due to vertically oriented ZnPP-tCsmA filaments, along the squeezing direction of the gel (Figure 2.8B), which indicates a predominantly parallel orientation of ZnPP planes to tCsmA scaffolds as well.[36-38] This is in line with the results of the 2D class average of filaments (Figure 2.8B). The lack of orientation for the 411 nm component is consistent with dissociation of the complex, which leads to a randomly oriented ZnPP fraction. The LD confirms that the binding of ZnPP to the tCsmA is necessary to build the supramolecular photosynthetic system.

Compared to the CD response of the monomeric ZnPP in propanol buffer, the B band of the complex at 430 nm shows a high intensity and nearly symmetric Cotton effect (Figure 2.2B). The strong CD signal observed is from ZnPP motifs interacting with each other and forming a chiral exciton coupled unit, with dipole-dipole interactions between monomers, which is well in line with Figure 2.7B, where the ZnPP appears to form tetrameric repeat units. In contrast, while the optical response for the ZnPP in propanol buffer in Figure 2.2A is stronger than for the complex, the CD is virtually absent, which confirms that the ZnPP in solution is monomeric. On the other hand, the CD response for the Q bands is very weak in the CD data collected from the complex. Since the LD data in Figure 2.7 are in line with a specific orientation angle of the ZnPP relative to the tCsmA scaffolds, and the particle shows a helical structure, the vanished dipole-dipole interaction of the Q bands indicates that the ZnPP possibly form oligomers with exciton coupling at a specific rotation angle in the molecular system to offset the dipole-dipole interaction of the Q bands.[39-41] Based on LD and TEM data, the ZnPP-CsmA complex probably forms a helical structure that is composed of twisted peptide assemblies built from well-ordered chiral oligomeric units that give rise to a single CD response (Figure 2.2B).[17, 41-44]

2.3.3 Photostability

The tCsmA-ZnPP complex forms large soluble particles that show a single distribution peak around 1.07 mL in the SEC data, with the retention

indicating a large molecular weight (Figure 2.9). This is consistent with the formation of extended filaments shown in the TEM data in Figure 2.7A. In addition, SEC also shows that the complex is quite sensitive to light. The peak shifts to ~ 1.09 mL after 30 minutes of light exposure, which indicates that the particle size became smaller upon exposure to light. Moreover, steady state fluorescence measurements indicate slow photo-dissociation of the complex upon illumination (SFigure 2.3). The histidyl axial binding of the ZnPP appears unstable under light exposure.[28] While free ZnPP precipitates in buffer, in the gel the ZnPP can be dissolved and in the LD data in Figure 4A a pronounced free ZnPP signal is observed at 411 nm wavelength, indicative of partial dissociation in the gel. Both the 430 nm and the 411 nm response decrease upon illumination, indicating photo-degradation for prolonged exposure, but the relative intensity changes in favor of the free ZnPP. With more than 2 h exposure with sunlight or 430 nm UV light, the complex was totally dissociated. The reason for the photo-dissociation might be that the dissipation of heat is slow.[15]

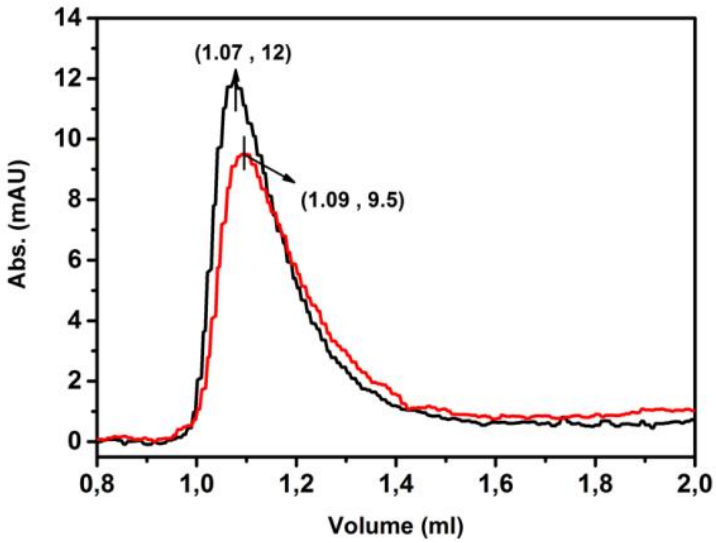

Figure 2.9 SEC elution spectra collected from the 50 µM tCsmA-ZnPP complex in pH 7.9, 50 mM KPi buffer (black trace) and the same sample after 30 minutes light exposure (red trace).

Despite photo-dissociation on longer time scales, the tCsmA-ZnPP complex is able to maintain a short time photostability. As Figure 2.10 shows, the stability is related to the concentration. At a concentration of about 20 µM the complex is stable for at least 30 minutes (Figure 2.10A). It has recently

been proposed that light-driven conformational changes in chiral protein scaffolds can develop vibronic states within or between linear arrays.[13] In such systems, excitons spread rapidly over the system, which may help to decrease the risk of damage and dissociation rate. However, during long time exposure the light still damages the complex which results in size decrease of the filament. Apparently a high concentration improves the stability, which suggests that distribution of energy helps to dissipate the excess energy and may be of vital importance for further improvement of the stability.

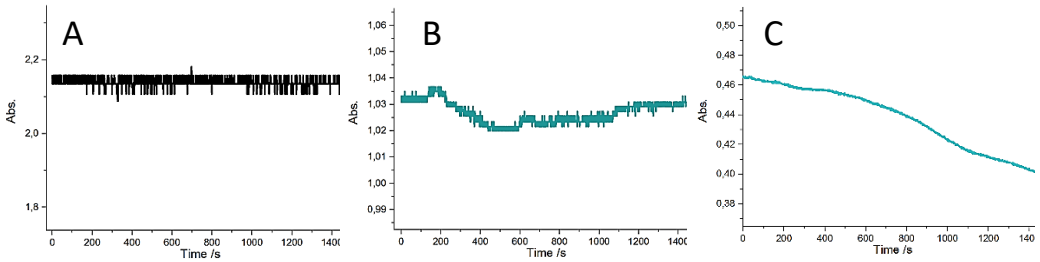

Figure 2.10 The photostability test by UV-Vis spectroscopy of the ZnPP-tCsmA complex with different concentration. A : 18 µM; B : 9 µM; C : 4.5 µM.

2.3.4 Exciton-energy transfer

To address further the energy transfer potential of the tCsmA-ZnPP self-assembly, an acceptor MV (SFigure 2.1) was added.[27-28, 45] Generally, MV exists in the dicationic form MV^{2+} (SFigure 2.1) in aqueous solution. However, MV has highly reversible redox reactions, at the reversible potential of E_0 = -0.4 ~ -0.55 V and -0.75 ~ -0.9 V vs NHE in aqueous solution.[26, 46-47] A solution of MV with sodium dithionite contains a mixture of MV^{+} and MV^{2+} (SFigure 2.5). When MV^{2+} is added to a suspension of tCsmA-ZnPP filaments in KPi buffer or the monomeric ZnPP in propanol buffer, fluorescence quenching is hardly observed (SFigure 2.6). This changes when the acceptor is converted to the cation radical form MV^{+} with excess sodium dithionite (SFigure 2.8).[48-51] As the data show, the tCsmA-ZnPP complex contains 594 nm and 650 nm emission peaks and the monomeric ZnPP contains 590 nm and 645 nm emission peaks after excitation (SFigure 2.6). On the other hand, the MV^{+} shows a strong broad absorption at 606 nm (ε = 13700 M^{-1} cm^{-1}), which overlaps with the tCsmA-ZnPP emission (SFigure 2.7A).[26] This leads us to conclude that intermolecular FRET or Dexter energy transfer between ZnPP and MV+ may cause fluorescence quenching by energy transfer. The

quenching is dependent on the concentration of MV^+. When the concentration was increased to about 300 µM MV^+ in the tCsmA-ZnPP solution, nearly all fluorescence of ZnPP was quenched (Figure 2.11).

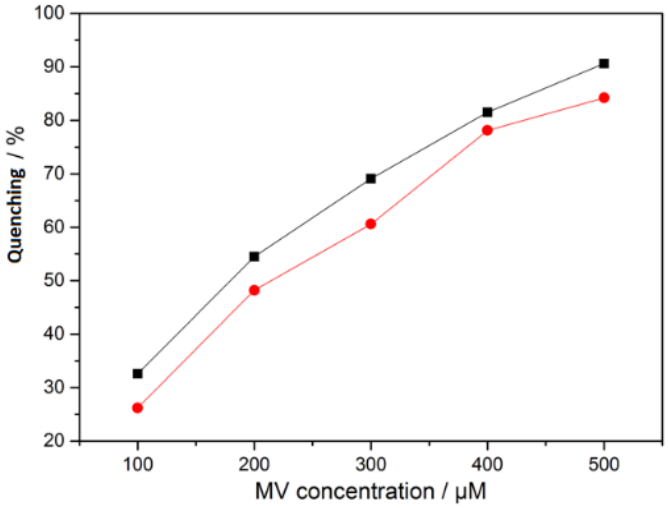

Figure 2.11 The fluorescence quenching diagram for 3.5 µM tCsmA-ZnPP complex at 594 nm (Black trace) and 650 nm, (Red trace) with different concentration of MV. The solution contains 1.25 mM sodium dithionite. The excitation wavelength is 440 nm.

Table 2.3 Fitted Time constants of Fluorescence Transients in tCsmA-ZnPP complex solution with different additives under a 440 nm excitation beam.

Additives	**594 nm Lifetime, ns**			
Lifetime	τ_1	τ_2	τ_3	$\tau_{average}$
No MV and $Na_2S_2O_4$	1.63 (9%)	0.5 (32%)	0.11 (59%)	0.37
MV^{2+} (no $Na_2S_2O_4$)	1.62 (8%)	0.63 (44%)	0.15 (48%)	0.48
MV^+ (excess $Na_2S_2O_4$)	1.1 (0.03%)	0.28 (0.12%)	0.001 (99.85%)	0.0017

Additives	**650 nm Lifetime, ns**			
Lifetime	τ_1	τ_2	τ_3	$\tau_{average}$
No MV and $Na_2S_2O_4$	3.13 (5%)	0.83 (29%)	0.14 (66%)	0.49
MV^{2+} (no $Na_2S_2O_4$)	2.82 (5%)	0.88 (44%)	0.21 (51%)	0.64
MV^+ (excess $Na_2S_2O_4$)	1.3 (0.01%)	0.4 (0.03%)	0.0015 (99.96%)	0.0017

As Table 2.3 shows, the exposure to the MV^+ acceptor reveals excellent energy transfer efficiency from the complex to the MV^+. The fluorescence decay responses at 594 nm and 650 nm can be described with 3 different lifetime components. All three lifetimes of the complex with the MV^+ additive are shortened, especially τ_3 was dramatically shortened to ~1 ps and the energy is almost 100% quenched by the acceptor. Although the time-resolved fluorescence spectroscopy has a limited resolution of 25 ps, τ_3 is about a few picoseconds or even shorter, at the femtosecond time scale. When sodium dithionite was depleted by letting it react with oxygen, the MV^+ was converted to MV^{2+} and there is no fluorescence quenching. The quenched complex recovered the same fluorescence as without acceptor, indicating that it maintains its integrity upon photoexcitation (SFigure 2.7). This highlights the importance of the MV^+ as the quenching species.

2.4 Conclusions

In conclusion, we have employed the dialysis method to gain control over metalloporphyrin forming an organized array with truncated CsmA peptides to develop helical scaffolds. The tCsmA-ZnPP complex forms soluble and stable long-aspect-ratio filaments to encapsulate strongly interacting oligomeric metalloporphyrins for photoexcitation. The solubility of the complex is good compared to the tCsmA starting material, which suggests that the amphipathic tCsmA has its hydrophobic residues on the inside and the hydrophilic residues on the outside. The tCsmA-ZnPP complex obtained by dialysis is well defined, and shows high purity. The single histidine available for binding with metalloporphyrin allows the material to get a stable 1:1 chromophore/peptide binding ratio. The self-assembly of the tCsmA-ZnPP complex shows certain photostability. The photoinduced energy of ZnPP-tCsmA complex can be transferred within few picoseconds with a nearly 100% quenching to MV^+. This artificial antenna system paves the way for the design of semisynthetic building blocks for light energy harvesting in artificial photosynthesis.

2.5 References

1. Chin, A. W.; Datta, A.; Caruso, F.; Huelga, S. F.; Plenio, M. B., *New Journal of Physics* **2010,** *12* (6), 065002.
2. Chin, A.; Prior, J.; Rosenbach, R.; Caycedo-Soler, F.; Huelga, S.; Plenio, M. B., *Nature Physics* **2013,** *9* (2), 113.
3. Huelga, S. F.; Plenio, M. B., *Contemporary Physics* **2013,** *54* (4), 181-207.
4. Pšenčík, J.; Ikonen, T.; Laurinmäki, P.; Merckel, M.; Butcher, S.; Serimaa, R.; Tuma, R., *Biophysical journal* **2004,** *87* (2), 1165-1172.
5. Adir, N., *Photosynthesis Research* **2005,** *85* (1), 15-32.
6. Van Grondelle, R., *Biochimica et Biophysica Acta (BBA)-Reviews on Bioenergetics* **1985,** *811* (2), 147-195.
7. van Grondelle, R.; Dekker, J. P.; Gillbro, T.; Sundstrom, V., *Biochimica et Biophysica Acta (BBA)-Bioenergetics* **1994,** *1187* (1), 1-65.
8. McConnell, I.; Li, G.; Brudvig, G. W., *Chemistry & biology* **2010,** *17* (5), 434-447.
9. Purchase, R.; de Groot, H., *Interface Focus* **2015,** *5* (3), 20150014.
10. Mathies, R. A., *Nature chemistry* **2015,** *7* (12), 945.
11. Yin, X.; Struik, P. C., *Journal of experimental botany* **2015,** *66* (21), 6535-6549.
12. Hoffman, D. P.; Mathies, R. A., *Accounts of chemical research* **2016,** *49* (4), 616-625.
13. R. Purchase, R. Cogdell, F. Breitling, V. Stadler, N. van Hulst, G.-J. Kramer, A. Ramirez, R. Zwijnenber, A. Kallergi (), J. B. de Baan, I. Rudra, and H. J. M de Groot *Bioinspired Chemistry* **2019**, 47-69.
14. Fry, H. C.; Garcia, J. M.; Medina, M. J.; Ricoy, U. M.; Gosztola, D. J.; Nikiforov, M. P.; Palmer, L. C.; Stupp, S. I., *J Am Chem Soc* **2012,** *134* (36), 14646-14649.
15. Luo, L.; Chang, C. H.; Chen, Y. C.; Wu, T. K.; Diau, E. W., *J Phys Chem B* **2007,** *111* (26), 7656-64.
16. Chromiński, M.; ó Proinsias, K.; Martin, E.; Gryko, D., *European journal of organic chemistry* **2013,** *2013* (8), 1530-1537.
17. Nielsen, J. T.; Kulminskaya, N. V.; Bjerring, M.; Linnanto, J. M.; Rätsep, M.; Pedersen, M. Ø.; Lambrev, P. H.; Dorogi, M.; Garab, G.; Thomsen, K., *Nature communications* **2016,** *7*, 12454.
18. Milks, K. J.; Danielsen, M.; Persson, S.; Jensen, O. N.; Cox, R. P.; Miller, M., *Photosynthesis research* **2005,** *86* (1-2), 113-121.
19. Zobova, A.; Taisova, A.; Lukashev, E.; Fedorova, N.; Baratova, L.; Fetisova, Z., *Journal of Biophysics* **2011,** *2011*.
20. Kulminskaya, N. V.; Pedersen, M. O.; Bjerring, M.; Underhaug, J.; Miller, M.; Frigaard, N. U.; Nielsen, J. T.; Nielsen, N. C., *Angew Chem Int Ed Engl* **2012,** *51* (28), 6891-5.
21. Zhou, Q.; Swager, T. M., *J Am Chem Soc* **1995,** *117* (50), 12593-12602.
22. Leonard, J. J.; Yonetani, T.; Callis, J. B., *Biochemistry* **1974,** *13* (7), 1460-1464.

23. Cogdell, R. J.; Gardiner, A. T.; Cronin, L., *Phil. Trans. R. Soc. A* **2012,** *370* (1972), 3819-3826.
24. Summers, L. A., *The bipyridinium herbicides*. Academic Press Inc.: 1980.
25. Bus, J. S.; Gibson, J. E., *Environmental health perspectives* **1984,** *55*, 37.
26. Watanabe, T.; Honda, K., *The Journal of Physical Chemistry* **1982,** *86* (14), 2617-2619.
27. Proux-Delrouyre, V.; Demaille, C.; Leibl, W.; Sétif, P.; Bottin, H.; Bourdillon, C., *J Am Chem Soc* **2003,** *125* (45), 13686-13692.
28. Komatsu, T.; Wang, R.-M.; Zunszain, P. A.; Curry, S.; Tsuchida, E., *J Am Chem Soc* **2006,** *128* (50), 16297-16301.
29. Kamlet, M. J.; Taft, R., *J Am Chem Soc* **1976,** *98* (2), 377-383.
30. Kodali, G.; Mancini, J. A.; Solomon, L. A.; Episova, T. V.; Roach, N.; Hobbs, C. J.; Wagner, P.; Mass, O. A.; Aravindu, K.; Barnsley, J. E., *Chemical science* **2017,** *8* (1), 316-324.
31. Milgrom, L. R.; Warren, M. J., **1997**.
32. Giovannetti, R., The use of Spectrophotometry UV-Vis for the Study of Porphyrins. In *Macro To Nano Spectroscopy*, InTech: 2012.
33. Montano, G. A.; Wu, H.-M.; Lin, S.; Brune, D. C.; Blankenship, R. E., *Biochemistry* **2003,** *42* (34), 10246-10251.
34. Li, Y.; Scales, N.; Blankenship, R. E.; Willows, R. D.; Chen, M., *Biochimica et Biophysica Acta (BBA)-Bioenergetics* **2012,** *1817* (8), 1292-1298.
35. He, S.; Scheres, S. H., *Journal of structural biology* **2017,** *198* (3), 163-176.
36. Furumaki, S.; Vacha, F.; Habuchi, S.; Tsukatani, Y.; Bryant, D. A.; Vacha, M., *J Am Chem Soc* **2011,** *133* (17), 6703-6710.
37. Abdourakhmanov, I. A.; Ganago, A. O.; Erokhin, Y. E.; Solov'ev, A. A.; Chugunov, V. A., *Biochimica et Biophysica Acta (BBA)-Bioenergetics* **1979,** *546* (1), 183-186.
38. Van Amerongen, H.; Vasmel, H.; Van Grondelle, R., *Biophysical journal* **1988,** *54* (1), 65-76.
39. Agranovich, V.; Galanin, M., *Electronic Excitation Energy Transfer in Condensed Matter* **1982**, 81-170.
40. Linnanto, J. M.; Korppi-Tommola, J. E., *The Journal of Physical Chemistry B* **2013,** *117* (38), 11144-11161.
41. Farid, T. A.; Kodali, G.; Solomon, L. A.; Lichtenstein, B. R.; Sheehan, M. M.; Fry, B. A.; Bialas, C.; Ennist, N. M.; Siedlecki, J. A.; Zhao, Z., *Nature chemical biology* **2013,** *9* (12), 826.
42. Pescitelli, G.; Gabriel, S.; Wang, Y.; Fleischhauer, J.; Woody, R. W.; Berova, N., *J Am Chem Soc* **2003,** *125* (25), 7613-7628.
43. Schellman, J. A., *Accounts of chemical research* **1968,** *1* (5), 144-151.
44. Harada, N.; Nakanishi, K., *Accounts of Chemical Research* **1972,** *5* (8), 257-263.
45. Tyson, D. S.; Luman, C. R.; Castellano, F. N., *Inorganic chemistry* **2002,** *41* (13), 3578-3586.
46. Steckhan, E.; Kuwana, T., *Berichte der Bunsengesellschaft für physikalische Chemie* **1974,** *78* (3), 253-259.

47. Bird, C.; Kuhn, A., *Chemical Society Reviews* **1981,** *10* (1), 49-82.
48. Kosower, E. M.; Cotter, J. L., *J Am Chem Soc* **1964,** *86* (24), 5524-5527.
49. Senn, D. R.; Carr, P. W.; Klatt, L. N., *Analytical biochemistry* **1976,** *75* (2), 464-471.
50. Bockman, T.; Kochi, J., *The Journal of Organic Chemistry* **1990,** *55* (13), 4127-4135.
51. MAYHEW, S. G., *European journal of biochemistry* **1978,** *85* (2), 535-547.

2.6 Appendix

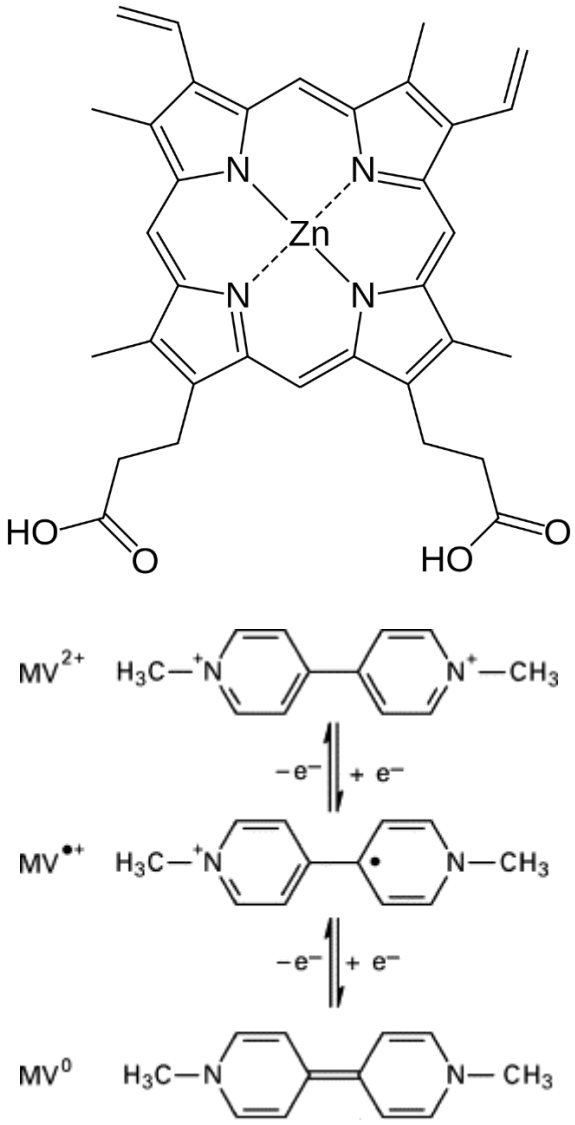

SFigure 2.1 The skeletal formula of zinc protoporphyrin and methyl viologen with different charge.

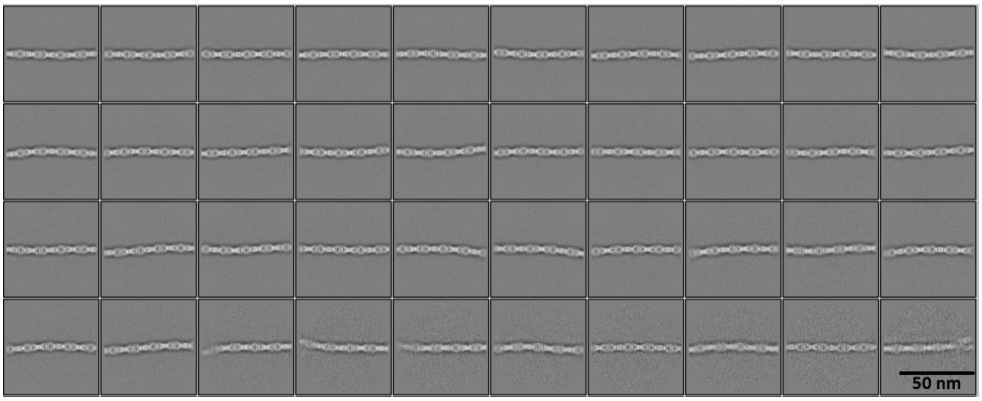

SFigure 2.2 50 classes 2D classification from 994142 particles by RELION2.0.

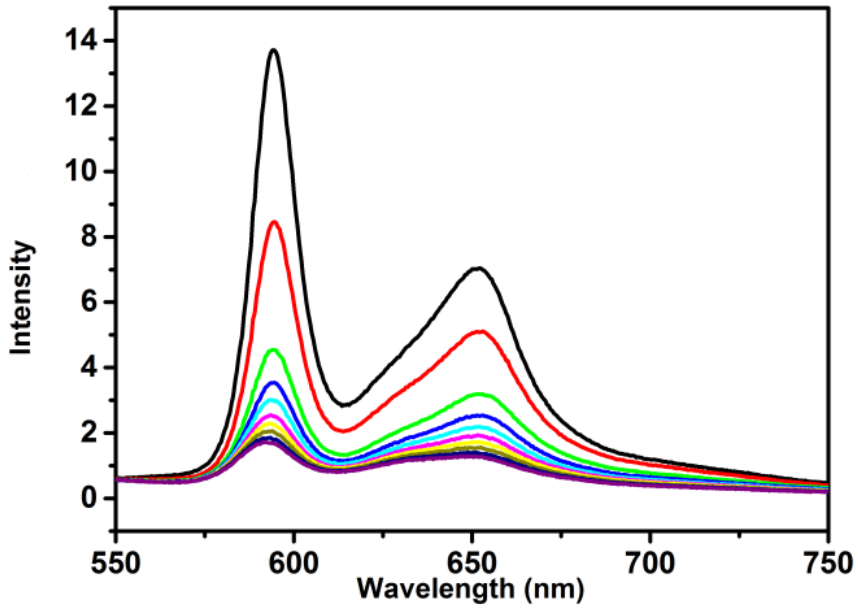

SFigure 2.3 Fluorescence spectroscopy of the tCsmA-ZnPP complex. The complex was excited at 430 nm for 5 minutes and followed 15 minutes incubation time. The concentration of the complex is 1.6 µM in pH 7.9 50 mM KPi buffer.

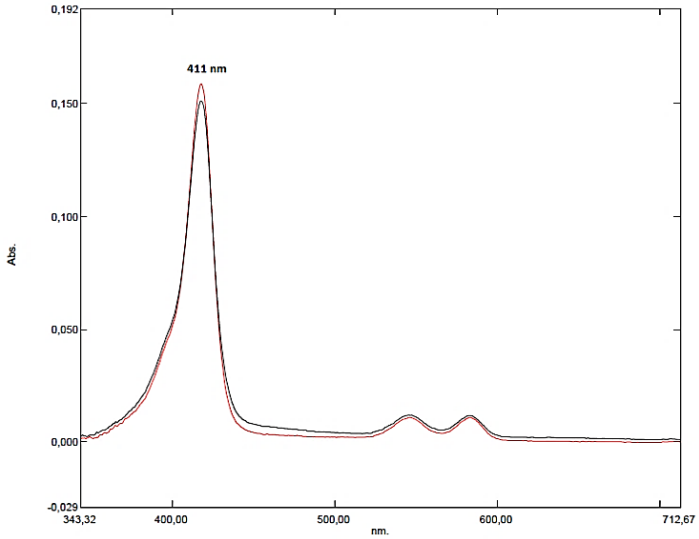

SFigure 2.4 UV-Vis spectra of the ZnPP-tCsmA complex after two hours in squeezing gel (black trace) and pure ZnPP (red trace) in squeezing gel. For both samples the major response is at 411 nm.

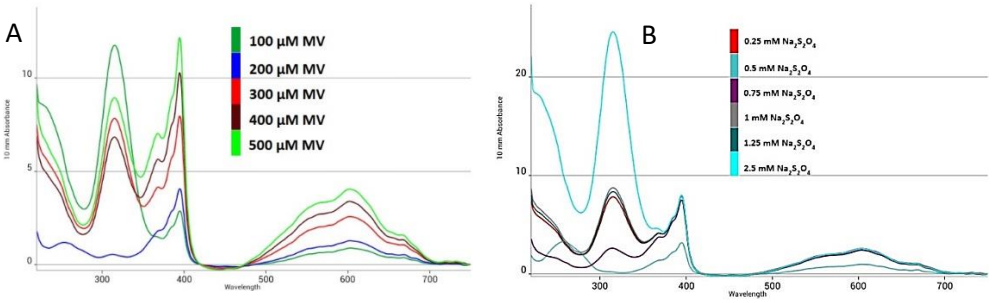

SFigure 2.5 A: the UV spectra of MV with different concentration with 1.25 mM sodium dithionite in the solution. The ratio of A396 nm/A606 nm is about 3 which is same as the ratio in spectra of MV^+. The peak at 606 nm is attributed to MV^+, whereas the peak 396 nm can be from MV^+ and MV^0. That means the sodium dithionite only converts MV to MV^+. If there is MV^0, the MV^0 will contribute to the UV absorption at 396 nm. In this case, the ratio A396 nm/A606 nm should be larger than 3. This reaction was also reported in the literature.[45] B: the UV spectra of 300 µM MV with different amounts of sodium dithionite. Adding more excess sodium dithionite does not improve the conversion rate. The MV can be saturated at about 60% conversion rate.

STable 2.1 The conversion rate of MV^+ (The concentration of sodium dithionite is 1.25 mM, ε606 nm of MV^+ is 13700 M^{-1} cm^{-1}), the data is from the results of SFigure 2.5B.

MV (µM)	Abs. 606 nm	MV^+ (µM)	MV^+/MV (%)	A396 nm/A 606
100	0.88	64	64	3.1
200	1.27	93	47	3.09
300	2.56	187	62	3.07
400	3.35	245	61	3.03
500	4.02	293	59	3.02

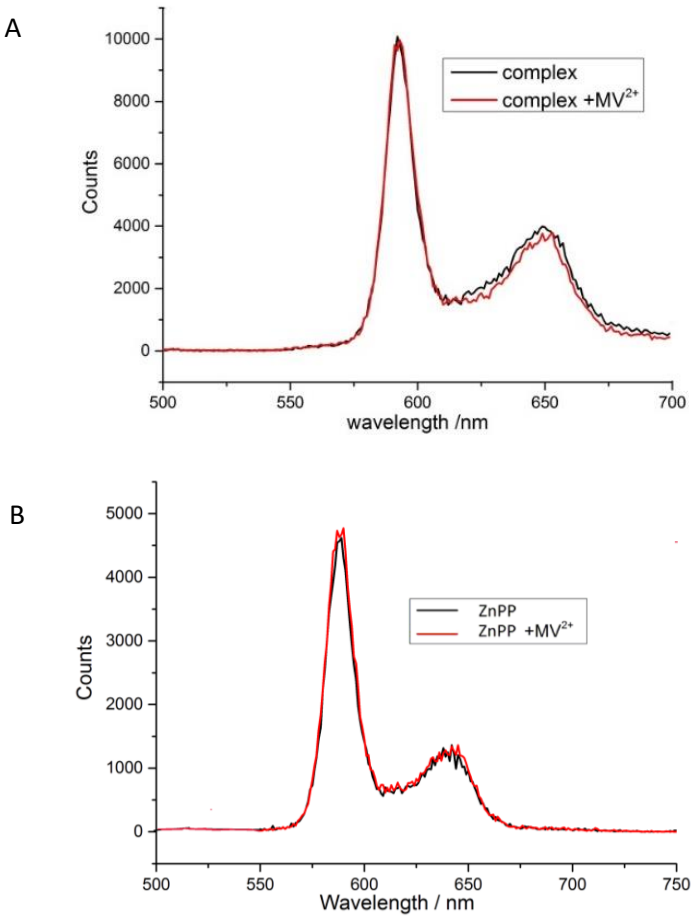

SFigure 2.6 A: Steady state fluorescence spectra of 4.5 µM tCsmA-ZnPP complex and 4.5 µM tCsmA-ZnPP complex with 500 µM MV in KPi buffer with 430 nm excitation light. B: Steady state fluorescence spectra of 10 µM ZnPP and 10 µM ZnPP with 500 µM MV in 6M 1-propanol KPi buffer with 416 nm excitation light.

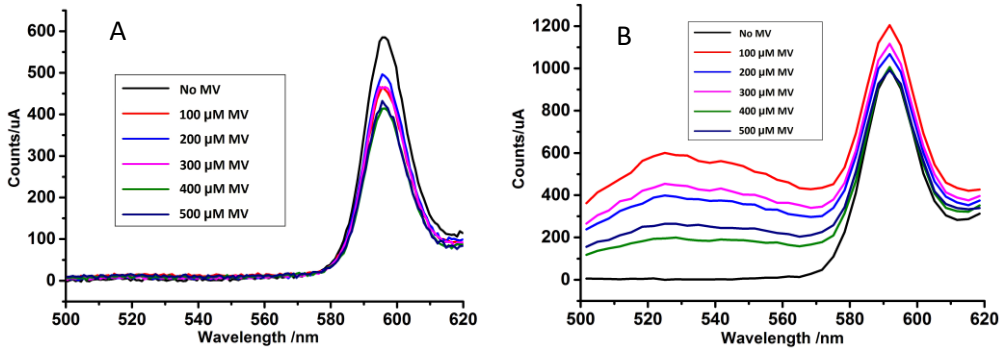

SFigure 2.7 A: Steady state fluorescence spectra of 3.5 µM tCsmA-ZnPP complex with different concentration of MV and the depleted 1.25 mM sodium dithionite in KPi buffer with 440 nm excitation light. B: Steady state fluorescence spectra of 3.5 µM ZnPP with different concentration of MV and depleted 1.25 mM sodium dithionite in 6M 1-propanol KPi buffer with 440 nm excitation light.

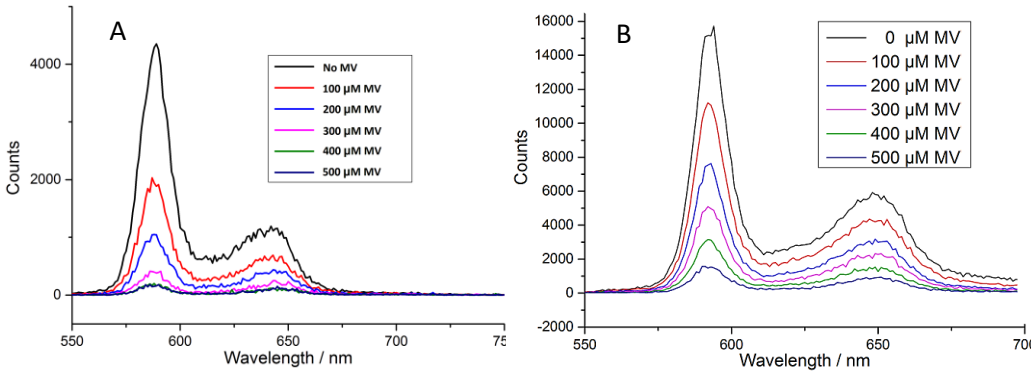

SFigure 2.8 A: Steady state fluorescence spectra of 3.5 µM tCsmA-ZnPP complex with different concentration of MV and 1.25 mM sodium dithionite in KPi buffer with 430 nm excitation light. B: Steady state fluorescence spectra of 10 µM ZnPP with different concentration of MV and 1.25 mM sodium dithionite in 6M 1-propanol KPi buffer with 416 nm excitation light.

STable 2.2 Preparation of the squeezing gel

Components	Volume (µL)
Glycerol (100%)	1500
37% (29:1) acrylamide	405
APS (10%)	30
TEMED	4.5
Complex (50 µM)	500
KPi buffer (3M, pH 7.9)	41.5
MQ water	519
Total	3000

STable 2.3 Fitted Time constants of Fluorescence Transients in monomer ZnPP solution with different additives under a 440 nm excitation beam.

Additives	590 nm Lifetime, ns			
Lifetime	τ_1	τ_2	τ_3	$\tau_{average}$
No MV and $Na_2S_2O_4$	2.767 (1.2%)	2.11 (98.8%)	-	2.12
MV^{2+} (no $Na_2S_2O_4$)	13.4 (0.1%)	2.12 (99.9%)	-	2.13
MV^{+} (excess $Na_2S_2O_4$)	22.65 (0.02%)	1.98 (99.98%)	-	1.98

Additives	645 nm Lifetime, ns			
Lifetime	τ_1	τ_2	τ_3	$\tau_{average}$
No MV and $Na_2S_2O_4$	2.94 (0.2%)	2.12 (99.8%)	-	2.12
MV^{2+} (no $Na_2S_2O_4$)	17.03 (0.02%)	2.12 (99.98%)	-	2.12
MV^{+} (excess $Na_2S_2O_4$)	10.94 (0.01%)	1.95 (99.99%)	-	1.95